Effects of Multiple Nozzles on Asymmetric Ejector Performance

D. Lineberry* and Dr. B. Landrum†
University of Alabama in Huntsville, Propulsion Research Center, Huntsville, AL 35899

This paper presents a comparison of a single nozzle and a dual nozzle strut based ejector. The results are focused on the fluid properties in the ejector duct. The research focused on choking mechanisms, mass flow entrainment, and mixing duct pressure distributions. The two ejectors were tested at equivalent primary mass flow rates. This corresponds to chamber pressures ranging from 100 psi. to 900 psi in the single nozzle strut and 50 psi to 450 psi in the dual nozzle strut. Secondary flow was drawn from the lab at atmospheric pressure, and was not controlled. The secondary flow was found to choke at a value of 2.3 lb/s for a primary mass flow rate of approximately 2.1 lb/s for both ejectors. This choke was believed to be a mass addition choke rather than a traditional aerodynamic choke. The mixing duct pressure distribution exhibited two distinct trends a "low pressure" trend and a "high pressure" trend. For the low pressure trend, the mixing length for the ejectors remained fixed around 20 inches, regardless of the chamber pressure. For the higher pressure trend, the mixing length was considerably longer and increased with increasing chamber pressure. At high chamber pressures (high mass flow rates), a supersonic core flow was present at the exit of the duct. For these cases, the two flow streams did not have time to mix by the end of the duct.

Nomenclature

A	=	Duct Cross Sectional Area
A_t	=	Nozzle Throat Area
M	=	Mach Number
m	=	Mass Flow
Ps	=	Static Pressure
Po	=	Stagnation Pressure
R	=	Air Specific Gas Constant
To	=	Stagnation Pressure
γ	=	Specific Heat Ratio

Subscripts

p	=	Primary Flow
s	=	Secondary Flow

I. Introduction

Combined Cycle Propulsion (CCP) technology shows promise for next generation launch vehicles.[1] Since a combined cycle engine incorporates several modes of engine operation into the same flow path, the optimum performance mode can be utilized in each flight regime. A typical Rocket Based Combined Cycle (RBCC) engine would operate in a rocket or ducted rocket mode for takeoff and initial acceleration to about Mach 2-3, transition to ramjet mode until Mach 4-6, and then transition to scramjet operation. Above Mach 6-8, scramjet operation is unrealistic, and the engine would operate as a pure rocket to accelerate into orbit.

---

*Graduate Research Assistant, Mechanical and Aerospace Engineering Department, S225 Technology Hall, Huntsville AL, 35899, Student Member
†Professor, Mechanical and Aerospace Engineering Department, S225 Technology Hall, Huntsville, AL, 35899, AIAA ~~Fellow~~ Associate Fellow (?)

The Strutjet[2] is one of the RBCC systems under consideration. This engine consists of a variable geometry duct with vertical engine struts mounted internally. Each strut has several rocket nozzles embedded within it. The engine operates in the four modes discussed earlier: ducted rocket, ramjet, scramjet, and pure rocket. In the airbreathing modes, atmospheric air is ingested into the inlet and flows between the struts into the mixing section. The air oxidizer is mixed with the fuel rich rocket exhaust and combusted. The combustion products are accelerated through an exit nozzle to provide the thrust.

A fundamental understanding of ejector physics is an enabling technology to realize an operational RBCC propulsion system. Past theoretical and experimental ejector studies have considered one-dimensional, axisymmetric, or at best two-dimensional geometries. Concepts such as the Strutjet use a complex asymmetric, three-dimensional flow path. The University of Alabama in Huntsville (UAH) Propulsion Research Center (PRC) has an ongoing research program to characterize asymmetric ejector performance in terms of mass flow entrainment and stream mixing. This study will help guide design of future RBCC systems and provide valuable data for validating computational fluid dynamic simulations of complex ejector systems.

II. Facility Description

The UAH PRC cold flow ejector facility was originally designed to approximate the flow path of the Aerojet Strutjet concept.[2] As shown schematically in Figure 1, the flow path consists of a rectangular cross section duct 4.5 in. wide by 3 in. tall. An elliptically contoured converging inlet is located on the front end of the duct to provide uniform airflow from the laboratory. A single strut is installed in the duct approximately 25 inches downstream of the inlet. The PRC has been experimenting with two struts, a single nozzle strut and a dual nozzle strut. The struts, shown in Fig. 2, have identical rectangular cross sections 1 inch wide by 7 inches tall. Rocket nozzles are embedded in the struts to provide the primary flow stream for the system. These nozzles have identical geometries with area ratios of approximately 4.66 and transition from a circular throat to a square exit. The dual nozzle strut also has a turbine exhaust slit approximately 0.094 in wide located between the two rocket nozzles. For this series of testing, the slit was not utilized, and was therefore filled.

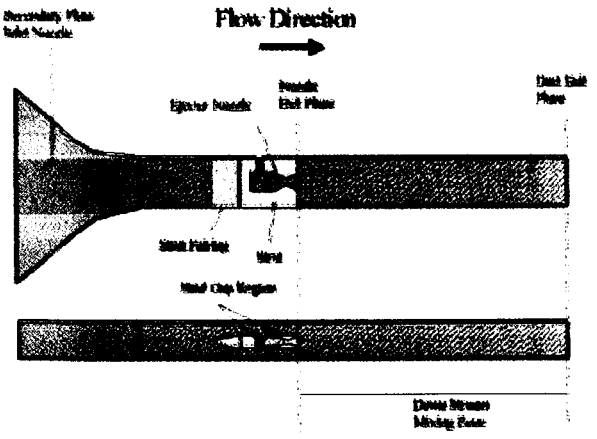

Figure 1. UAH Strut Ejector Flow Path (Not to Scale)

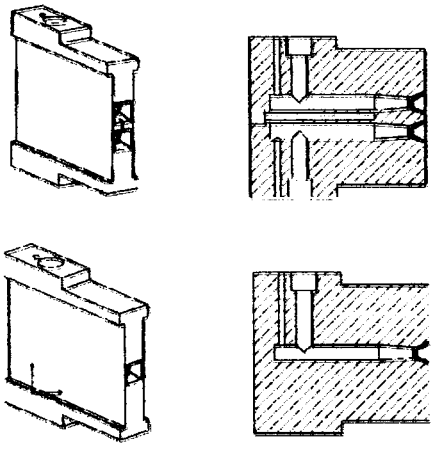

Figure 2. CAD Drawings of Dual and Single Nozzle Struts

The PRC ejector facility is shown in Fig. 3. The facility consists of two air tanks with a combined volume of 524 cubic feet, 1.25 in. stainless steel supply tubing, a PID controller to regulate chamber pressure, and the duct. A single strut is installed in the duct for a particular test. The duct exits into a constant area sheet metal diffuser that is open to the laboratory. An array of 48 static pressure taps are located along the centerlines of the top and side walls of the duct. The taps are spaced 0.5 inches apart for the first 10 inches, and 1.0 inch apart for 28 inches that follow. Ten static pressure taps are located on the centerline of the sidewall in the strut gap region of the duct. This region is located upstream of the rocket nozzle exit plane between the strut and the sidewall of the duct (see Figure 1). An aerodynamic fairing is located on the upstream end of the strut to provide uniform flow in the strut gap region. A Pitot-static probe is embedded in this fairing to measure the stagnation and static pressure of the secondary (induced) flow. A Pitot-static probe is also located at the exit plane of the duct. This probe measures the stagnation and the

static pressure of the presumed fully mixed flow at the exit of the duct. The probe is mounted to a traversing mechanism, so the pressure can be recorded at various positions across the exit plane.

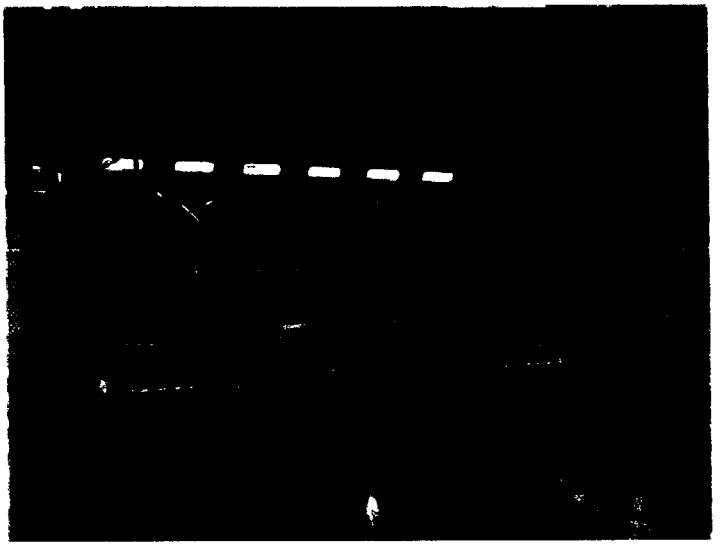

Figure 3. UAH PRC Ejector Facility

A pressure tap is also located in the chamber of the rocket nozzle to measure the chamber pressure of the rocket. The chamber pressure measurement is connected to a feedback loop of the PID controller to maintain a relatively constant chamber pressure for the experiment. In addition to the pressure instrumentation of the duct, two thermocouples are located in the duct. One measures the temperature of the rocket chamber, and the other measures the temperature of the secondary air stream. An outside barometer/thermometer is used to measure the atmospheric pressure and temperature in the lab at the time of each test.

III. Previous Research

The UAH PRC has an ongoing research program to characterize asymmetric ejector performance and fluid mechanics. The initial studies were focused on the mixing between the rocket and turbine exhausts with the ingested air[3-5] using laser induced florescence for flow visualization. The study examined the mixing as a function of the ratio of chamber pressure to turbine exhaust pressure. A complimentary study was performed to examine the rocket induced flow field in the rectangular duct for the dual nozzle strut.[6] The induced airflow as a function of primary rocket flow rate was measured. Pitot pressure traverses were used to examine the expansion rate of the rocket and turbine exhaust plumes, and assess mixing losses. Pressure traverses were also made in the strut gap region where the secondary flow choke was believed to occur. At the time of these studies, the instrumentation was limited.

The facility was refurbished after this initial series of tests. Additional pressure taps were added along the top and sidewalls of the mixing duct and in the strut gap region. A series of tests on the single nozzle strut were performed to examine details of the choking and mixing process.[7,8] This work was recently extended to higher pressures and was presented at the 2003 Joint Propulsion Conference.[9] Reference 9 included data from a limited number of tests. This paper presents data from additional single nozzle tests, as well as a complete set of dual nozzle tests.

IV. Test Procedure

For each test series, the storage tanks are pressurized to 2500 psi to ensure that a complete set of chamber pressures can be tested. When the test begins, the chamber pressure of the rocket nozzle is established at one of the desired (set) pressures, and measurements are taken along the duct. When ten measurements of each of the top wall and sidewall pressure taps have been taken, the chamber pressure is ramped up or down to the next set pressure. Tests have been performed in steps of increasing chamber pressure and in steps of decreasing chamber pressure to

assess any hysteresis effects. For tests examining the mixing duct pressure distribution, the test is run for a period of time long enough for 10 measurements to be taken at each of the 48 pressure taps along the top and side wall. A mechanical scani valve is used to record pressure measurement at a given tap and then move to the next postion along the mixing duct. Each tests requires approximately 2 minutes of flow time to complete the 10 cyles. For the pressure distribution, mass flows, Mach number, and strut gap pressure results, the data presented consist of average values from ten separate tests. For pressure traverses across the exit, traces were taken at five different locations from the centerline to the top wall. The traverses consist of movement from the center of the duct to the side wall. The probe was stopped in 11 distinct locations and took 15 measurements at each stop. This data was then averaged at each position, to create the plot.

V. Results

A. Mass Flow

For RBCC applications, the secondary flow mass entrainment is a critical aspect of the air breathing portions of flight. The mass flow of the secondary air as a function of chamber pressure is critical in establishing mixture ratios for engine operation and the amount of onboard oxidizer that will be required. For the current experimental apparatus, secondary mass flow is calculated from the stagnation and static pressures measured by a Pitot-static probe upstream of the strut, and from the inlet temperature of the flow. With the area of the duct at the measurement locations known, the mass flow is calculated according to

$$\dot{m}_s = \sqrt{\frac{\gamma}{R}} \cdot \frac{P_s}{\sqrt{T_{os}}} \cdot A \cdot \sqrt{\left(\frac{P_{os}}{P_s}\right)^{\frac{\gamma-1}{\gamma}} \cdot \frac{2}{\gamma-1} \cdot \left(\left(\frac{P_{os}}{P_s}\right)^{\frac{\gamma-1}{\gamma}} - 1\right)} \tag{1}$$

This equation is based on idealized flow. Geometry effects of the rectangular duct inlet are not included. The mass flow of the primary stream is calculated based on the assumption that the flow is choked at the throat of the rocket nozzle using the equation

$$\dot{m}_p = \frac{P_{op}}{\sqrt{T_{op}}} A_t \sqrt{\frac{\gamma}{R}\left(\frac{2}{\gamma+1}\right)^{\frac{\gamma+1}{\gamma}}} \tag{2}$$

where the chamber pressure is specified for the test, and the chamber temperature is measured by a thermocouple in the rocket chamber. Figure 4 shows the variation of both primary mass flow and secondary mass flow plotted against the chamber pressures for both the single and dual nozzle strut.

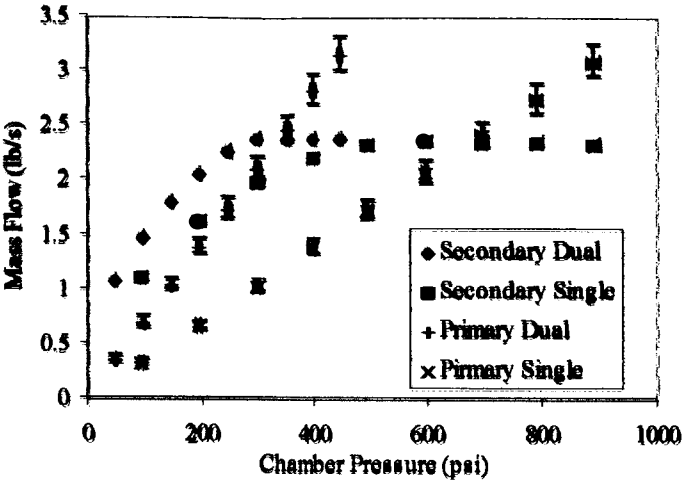

Figure 4 Secondary and Primary Mass Flow (Dual and Single Nozzle)

As can be seen in the figure, the secondary flow for both the single and dual nozzle appears to reach a maximum at a mass flow of around 2.4 lb/s. For the single nozzle this occurs at a chamber pressure of approximately 600 psi, for the dual nozzle, this occurs around 300 psi. Since the nozzle exit area for the dual nozzle is twice that of the dual nozzle, the maximum secondary flow occurs around the same primary mass flow for both struts. This corresponds to a primary mass flow of appriximately 2.1 lb/s. This can be seen more clearly in Figure 5, which shows the secondary mass flow plotted agianst primary mass flow for both nozzles.

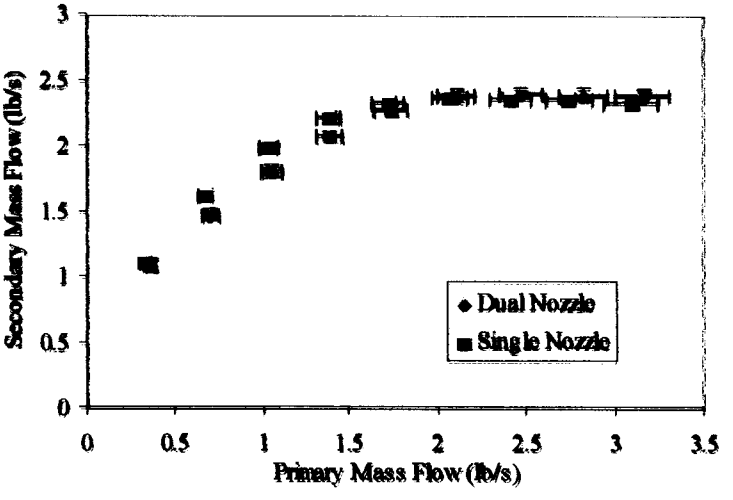

Figure 5 Secondary Mass Flow versus Primary Mass Flow (Dual and Single Nozzle)

Figure 5 indicates that the maximum secondary mass flow occurs near the same primary mass flow. This indicates that the secondary flow is a function of momentum rather than exit pressure of the nozzle. The choke which occurs is more likely a mass addition choke than a geometric choke as identified by Fabri[10]. Also noticeable in Figure 5 is that the secondary flow for the dual nozzle is in general slightly less than that of the single nozzle for the same primary mass flow rate until the choke is reached.

Mass flow entrainment is another important parameter in RBCC applications. This quantity is the amount of secondary flow that can be induced for a given primary mass flow. Figures 6 and 7 show mass flow entrainment using a parameter called the suction ratio, which is calculated by

$$\omega = \frac{\dot{m}_s}{\dot{m}_p} \tag{3}$$

where $\dot{m}_s$ is the secondary mass flow and $\dot{m}_p$ is the primary mass flow. Figure 6 shows the suction ratio plotted against the ratio of the nozzle chamber pressure to the secondary flow stagnation pressure (atmospheric pressure). Figure 7 shows the suction ratio plotted against primary mass flow rate.

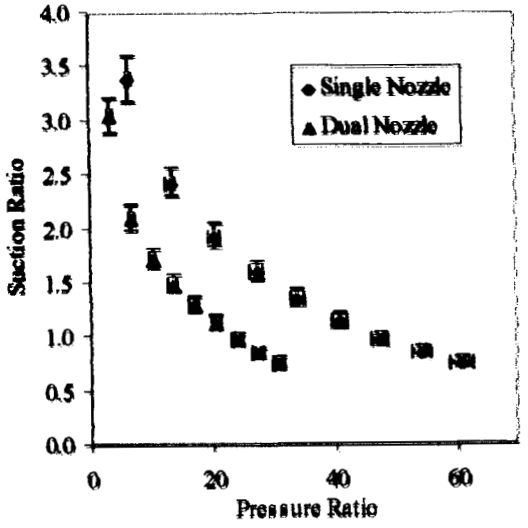

Figure 6 Suction Ratio Versus Pressure Ratio (Single and Dual Nozzles)

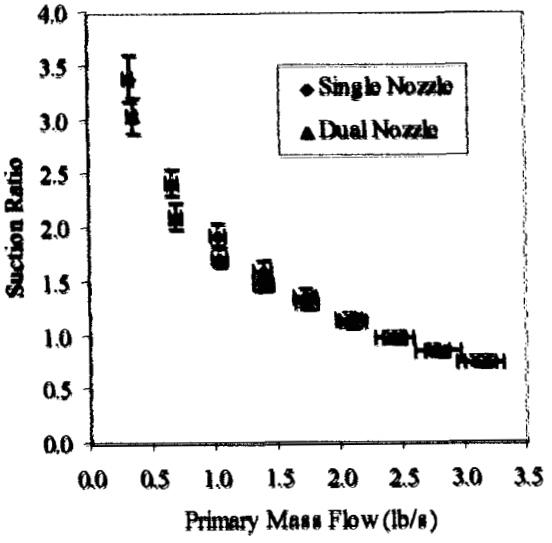

Figure 7 Suction Ratio Versus Primary Mass Flow (Single and Dual Nozzles

B. Mach Numbers

The Mach number of the secondary flow upstream of the strut and the presumed mixed flow at the exit of the duct were next evaluated. Total and static pressures were measured upstream of the strut for the secondary flow and in the center of the duct exit for the mixed flow. The resultant Mach numbers were determined from the ratios of the measured total and static pressures. Two separate equations must be used depending on whether the flow is sonic or subsonic. For the subsonic flow ahead of the strut the Mach number M is calculated by

$$M_s = \sqrt{\frac{2}{\gamma - 1}\left(\left(\frac{Po_s}{P_s}\right)^{\frac{\gamma-1}{\gamma}} - 1\right)} \tag{4}$$

where Pos is the stagnation pressure measured by the Pitot probe, Ps is the static pressure measured by the probe, and γ is the ratio of specific heats (equal to 1.4 for air).

The duct exit flow could be subsonic or supersonic. When the flow is subsonic Eq. (4) is used. When the flow is supersonic, then a shock will form in front of the blunt probe. The stagnation pressure measured by the probe will be total pressure on the downstream (subsonic) side of the shock wave (Po2). For such a case the free stream flow Mach number (M_1) is derived from the pressure measurements by using

$$\frac{Po_2}{P_1} = \left[1 + \frac{2\gamma}{\gamma+1}\left(M_1^2 - 1\right)\right] \cdot \left[1 + \frac{\gamma-1}{2}\left(\frac{1 + \frac{\gamma-1}{2}M_1^2}{\gamma \cdot M_1^2 - \frac{\gamma-1}{2}}\right)\right]^{\frac{\gamma}{\gamma-1}} \quad (5)$$

In this equation, P_1 is a static pressure measured on the upstream (free stream) side of the shock. In the present experiments, a static pressure on the sidewall of the duct at the exit plane is used for the static pressure, and the stagnation pressure is measured with a Pitot probe in the center of the exit plane. To pick which equation is required, the ratio of the stagnation pressure to static pressure is determined. If this ratio is less than 1.89, then the flow is subsonic, and Eq. (4) is used. If the pressure ratio is greater than 1.89, then the flow will be sonic, a shock will form in front of the probe, and Eq. (5) must be used.

Figure 8 shows the Mach numbers of the secondary flow and the mixed flow at the duct exit for both the single and dual nozzle struts at each of the studied chamber pressures. For all tests the secondary flow Mach number reached a constant value of approximately 0.28 at a primary chamber pressure of approximately 600 psi for the single nozzle strut and a chamber pressure of approximately 300 psi for the dual nozzle strut. This is consistent with the secondary mass flow choking indicated in Figs. 4 and 5. For the single nozzle strut, the Mach number at the duct exit increased to a value of approximately 0.625 where it began to level off around a chamber pressure of 600 psi. As chamber pressure increased further, the Mach number began to increase again. For chamber pressures of 800 and 900 psi the exit pressure measurements indicated that the flow was supersonic. For the dual nozzle strut, the same trend appears. The exit Mach number remains subsonic for chamber pressures of 350 of lower. Although the data does not appear to level off as the single nozzle does, the plot shows a jump to supersonic flow for chamber pressures above 400 psi. The mixing duct pressure profiles shown later will indicate this is because the secondary flow has not fully mixed with the supersonic core of the primary jet at these conditions.

Figure 9 shows the inlet and exit Mach numbers plotted against primary mass flow. Again, as noted earlier, an equivalent primary mass flow for the dual nozzle strut corresponds to half the chamber pressure in the single nozzle strut. In the figure it is evident that the secondary flow chokes at a mass flow of approximately 2.3 lb/sec for both the dual and single nozzle. In Figure 9, it can also be seen that the flow goes from subsonic to supersonic at approximately the same primary mass flow rate. This indicates that the momentum effects present in the ejector system are the driving influence in the flow features and the pressure effects have less impact. The highest mach number reached for the dual nozzle flow was approximately 1.3, while the highest mach number for the single nozzle strut was approximately 1.1.

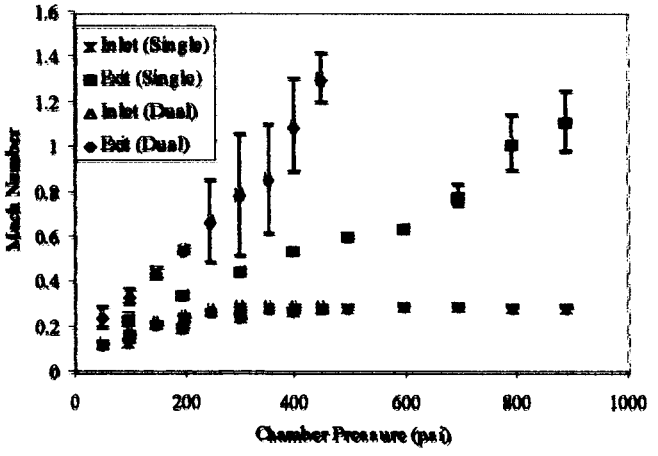

Figure 8 Inlet and Exit Centerline Mach Numbers versus Chamber Pressure (Single and Dual Nozzles)

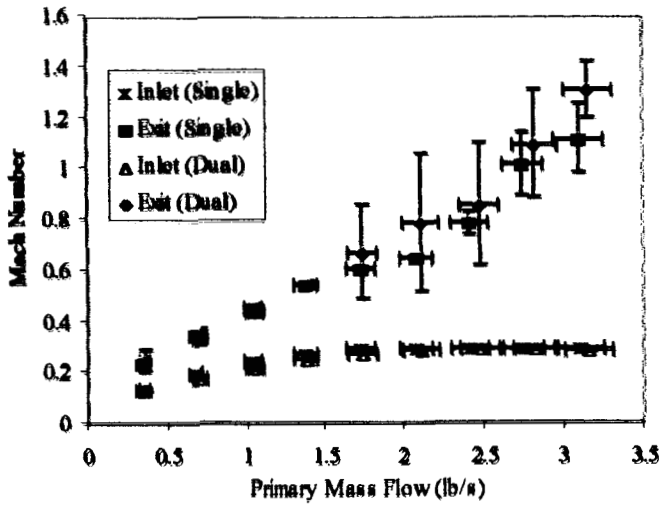

Figure 9 Inlet and Exit Centerline Mach Number Versus Primary Mass Flow (Single and Dual Nozzles)

C. Strut Gap Pressures

While the plots of Figures 4 and 5 and Figures 8 and 9 indicate that the secondary flow becomes choked, these plots do not indicate the type of choke which occurs. In a confined ejector system like the facility at the PRC there are two primary means of choking the secondary flow as shown in Fig. 10. When a flow is restricted by a minimum geometric area (such as the throat of a nozzle), it may choke at that point. The maximum mass flow that may pass down the duct is limited to the maximum mass flow that may pass through that restriction. This type of choke is referred to as an aerodynamic choke. The other type of choke, a mass addition or Fabri choke[10,11], is caused by the restricting of the secondary flow between the outer duct wall and the expanding plume of the primary jet. The secondary flow is still not fully mixed with the primary flow and is acting independently. The plume boundary acts as a wall for the secondary flow and the maximum mass flow for the stream is that which can pass through the area created by the wall and the plume boundaries.

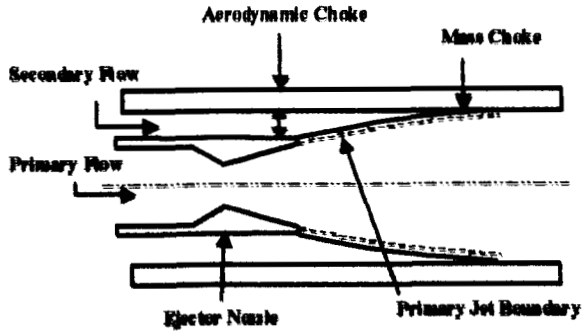

Figure 10 Choking Mechanisms in a Confined Ejector System

In order to determine the type of choking mechanism for the UAH ejector facility, the secondary flow static pressures in the minimum geometric area of the strut gap were examined. If the choke is an aerodynamic choke it will occur in the strut gap region. Figures 11 and 12 show the ratio of the wall static pressure to the secondary flow total pressure at each of the ten pressure tap locations in the strut gap. All of the chamber pressures tested are shown on the plots.

Because of the scale of the plots and the proximity of several sets of data, uncertainty bars are not shown. The uncertainties for these data points range from 0.5% to 3.5%. The dashed line in the figures shows the sonic limit (Ps/Pos = 0.528 for $\gamma = 1.4$). A pressure ratio at or below this point would indicate the presence of an aerodynamic choke.

Initially, as the chamber pressure is increased, the strut gap pressure ratio decreases and approaches the sonic limit. When the chamber pressure reaches a value of around 600 psi (single nozzle) and 350 psi (dual nozzle), the pressure ratio begins to increase (away from the sonic limit). This movement away from the sonic limit would indicate that the flow in the strut gap is not choked in this region at these higher pressures.

Figures 11 and 12 show pressure ratios measured in the two tests of Figs. 9 and 10 for chamber pressures between 500 and 980 psi. The plot scale is expanded and uncertainty bars have been added. As can be seen, the plots become very congested when uncertainty bars are shown. These plots indicate the flow is approaching an aerodynamic choke in the strut gap region when for chamber pressures around 650 psi. However, as the chamber pressure is increased beyond 650 psi, the pressure ratio obviously begins to increase away from the sonic limit. At the highest chamber pressures of each figure the secondary pressure ratio is well above the sonic ratio suggesting that an aerodynamic choke does not occur in the strut gap region. These results indicate a complex change in flow behavior when the driving primary jet pressure increases between 600 and 700 psi. The mixing duct pressures were next evaluated to help clarify this phenomena.

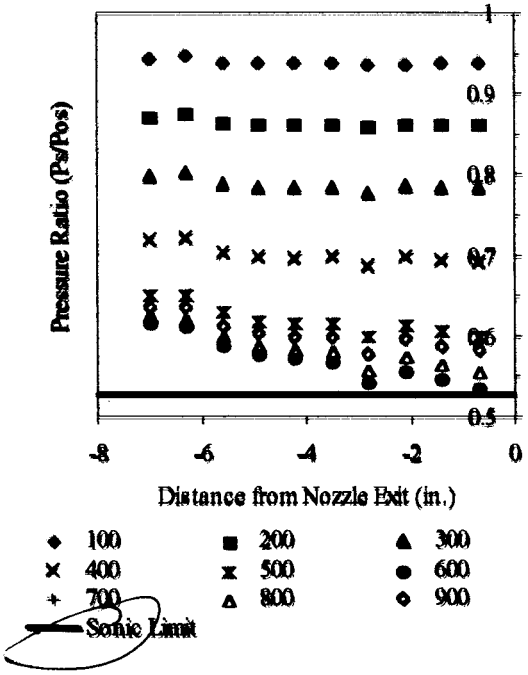

Figure 11 Single Nozzle Strut Gap Pressure Ratios

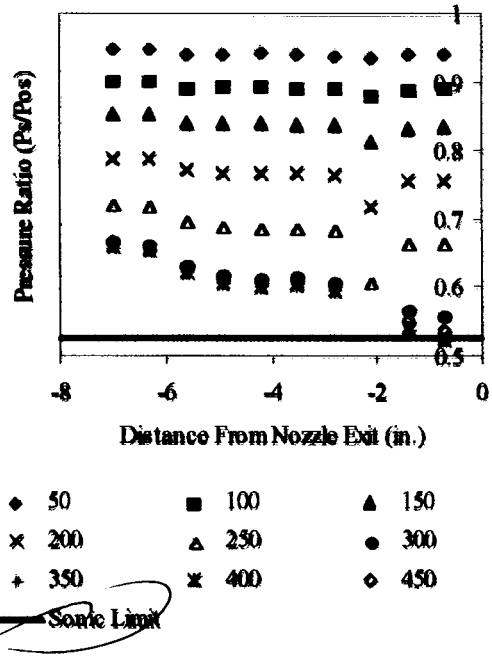

Figure 12 Dual Nozzle Strut Gap Pressure Ratios

For each chamber pressure and for both nozzles, the pressure ratio drops as the flow approaches the nozzle exit plane. From a test to test stand point, as the chamber pressure is increased, the strut gap pressure ratio decreases and approaches the sonic limit. When the chamber pressure reaches a value of around 650 psi, the pressure ratio begins to increase (away from the sonic limit). This movement away from the sonic limit would indicate that the flow in the strut gap is not choked at these higher pressures.

Figures 13 and 14 shows pressure ratios measured for the single nozzle strut at chamber pressure set points between 500 psi and 900 psi and for the dual nozzle strut at chamber pressure set points between 250 psi and 450 psi. The plot scales are expanded. These plots indicate the flow is approaching an aerodynamic choke in the strut gap region for chamber pressures around 650 psi (single nozzle) and 350 psi (dual nozzle). However, as the chamber pressure is increased above these values, the pressure ratio obviously begins to increase away from the

sonic limit. At the highest chamber pressures of each figure the secondary pressure ratio is well above the sonic ratio suggesting that an aerodynamic choke does not occur in the strut gap region. For the Dual Nozzle Fig. 14, the pressure ratio appears to reach the sonic limit in the strut gap region, however the movement away from this pressure limit at higher chamber pressures, while the mass flow remains constant (Fig. 4) indicates that an aerodynamic choke is not present in this region. The uncertainty bars (if shown) would indicate that the true value may be above the sonic limit. These results do however; indicate a complex change in flow behavior when the driving primary jet pressure increases. The mixing duct pressures were next evaluated to help clarify these phenomena.

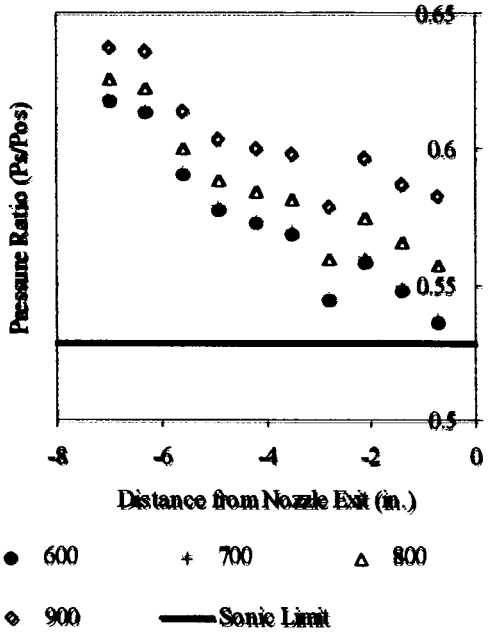

Figure 13 Single Nozzle Strut Gap Pressure Ratios (Higher Chamber Pressures Only)

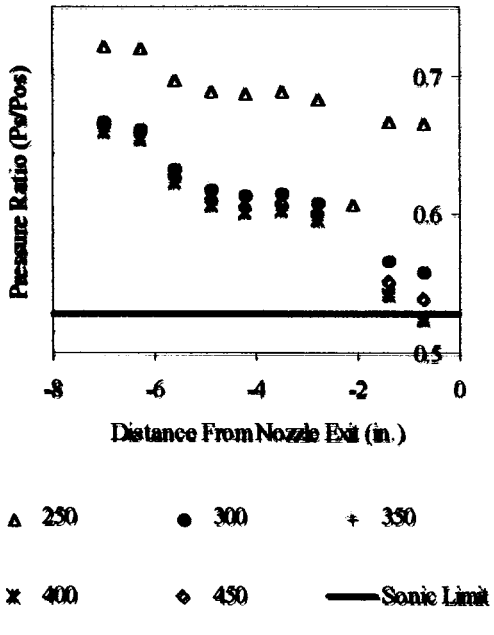

Figure 14 Dual Nozzle Strut Gap Pressure Ratios (Higher Chamber Pressures Only)

D. Mass Flow Calculations

Figure 4 indicated that the secondary flow becomes choked around a pressure of 500 psi for the single nozzle and 250 psi for the dual nozzle At these point Figs. 11-14 indicate that the secondary pressure ratios in the strut gap are not within the sonic limit. This suggests that the secondary flow choking must be a mass addition choke in the mixing duct downstream of the strut. As chamber pressure is increased, there is little to no observable change in the secondary mass flow rate. This trend alone does not conclusively prove that the choke does not change from a mass flow choke to an aerodynamic choke. However, if it is assumed that an aerodynamic choke occurs in the strut gap, the mass flow rate can be estimated from the secondary flow stagnation temperature and pressure according to the classical one-dimensional, ideal flow equation

$$\dot{m} = Po_s \cdot A \cdot \gamma \frac{\sqrt{\left(\frac{2}{\gamma+1}\right)^{\frac{\gamma+1}{\gamma-1}}}}{\sqrt{\gamma \cdot R \cdot To}} \qquad (6)$$

where A is the cross sectional area of the strut gap region. Based a secondary flow total pressure of approximately 14.7 psi, Eq. (6) produces a maximum mass flow of 3.2 lbm/s for the secondary flow stream. Figure 4 indicates that the secondary mass flow chokes with a mass flow equal to 2.3 lbm/s.

Equation (6) is an idealized equation that yields an order of magnitude value. It neglects many aspects of the flow which may lower the estimates of mass flow such as boundary layers, non-uniform velocity profiles, thermal, and viscous effects. The mass flow rates shown in Figs. 4 and 5 are also idealized to some extent. The Pitot-static pressure ratios were measured on the duct centerline and used to calculate a Mach number. The secondary flow was assumed to be incompressible based on the resultant calculated Mach numbers that were less than 0.3 (see Fig. 7). The density and temperature of the secondary flow to this point were assumed to be constant. The temperature was used to calculate a speed of sound. The speed of sound was then used to calculate velocity from Mach number. Finally, the secondary mass flow rate was determined from velocity and density.

Although the incompressible flow assumption seems reasonable, there is an unknown velocity profile across the duct. The calculated secondary mass flow rate is based on the maximum centerline velocity and is thus somewhat larger than the actual value. Even if the non-ideal nature of the duct flow is accounted for, the experimentally determined mass flow rate is approximately 2/3 of the theoretical value required for an aerodynamically choked flow. Although the strut gap pressure ratios indicate slightly inconsistent results, it is believed the secondary flow choking is most likely due to a mass choke downstream of the rocket exit plane rather than an aerodynamic choke in the strut gap.

E. Mixing Section Static Pressures

Static pressure measurements along the centerlines of the top and side walls of the duct downstream of the strut exit plane are used to evaluate mixing of the primary and secondary flow streams. Figure 15 shows a plot of the top and sidewall pressures for the single nozzle strut at a chamber pressure of 200 psi. Figure 16 shows a plot of the mixing duct pressure distribution for the dual nozzle strut at 100 psi chamber pressure (mass flow comparable to 100 psi in the single nozzle strut). The pressures in the figure have been normalized by dividing by the secondary flow total pressure at the inlet (the lab atmospheric pressure).

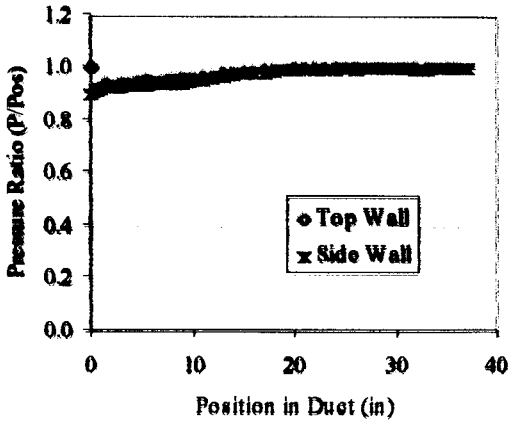

Figure 15: Mixing Duct Pressure Distribution Single Nozzle Strut (Pc = 200 psi)

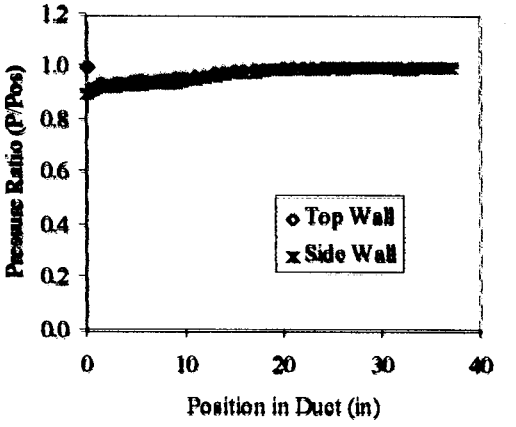

Figure 16 Mixing Duct Pressure Distribution Dual Nozzle Strut (Pc = 100 psi)

As can be seen in both figures, the side wall pressure at the nozzle exit starts at a value approximately equal to the last strutgap pressure ratio, then gradually recovers. In both cases, pressure has recovered between 15 to 20 inches downstream. The top wall pressure trace shows that initially near the base of the strut there is a region of high pressure as the secondary flow tries to turn the corner around the strut. This is believed to be a region of separated flow. Approximately 0.5 inches downstream of the exit plane, the top wall pressure drops sharply to match the sidewall pressure and then begins a gradual recovery until it reaches a pressure ratio value near 1 at between 15 to 20 inches downstream of the exit plane. These trends were common in both single and dual nozzle plots for the lower chamber pressures tested (100 to 500 psi for the single nozzle, and 50 to 250 psi for the dual nozzle). For all of these lower pressures, the recovery location varied little. Top and side wall pressures recovered between 15 to 20 inches downstream of the nozzle exit plane. However, the magnitude of the initial pressure drop increased with increasing chamber pressure. The pressure traces of the top and sidewall track each other very well. The flow is considered to be fully mixed at the point where the two pressures equalize with atmospheric pressure, approximately 25 inches downstream.

For higher chamber pressures, Pc > 600 psi (single) and Pc >300 psi (dual) the pressure distribution plots showed a different trend. Figures 17 and 18 show the mixing duct pressure distributions for the single nozzle at a chamber pressure of 800 and for the dual nozzle at a chamber pressure of 400 psi respectively.

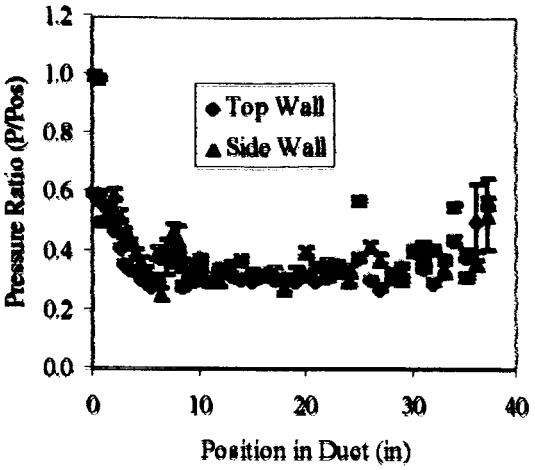

Figure 17 Single Nozzle Mixing Duct Pressure Distribution (Pc = 800 psi)

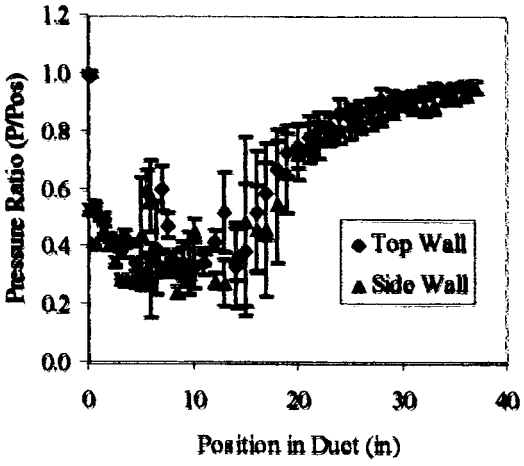

Figure 18 Dual Nozzel Mixing Duct Pressure Distribution (Pc = 400 psi)

In Figures 17 and 18, the sidewall pressure ratio continues to decrease after passing the strut exit plane and then reaches a region of approximately stable pressure with some pressure discontinuities due to flow structure, then begins to recover farther downstream. But the mixing length for these higher chamber pressures is considerably longer than for the lower pressure cases. In both figures, the top and sidewall pressures do not equalize with atmospheric pressure by the end of the duct. This is an indication of poor flow mixing in the duct. The region of separation within the first half inch of duct downstream of the strut is still visible in the first two measurements of the top wall pressure trace. In Figure 17, the pressures have just started to recover, however for the dual nozzle strut at the same mass flow (Figure 18) the pressure begins to recover around 15 in. downstream of the strut exit. Additionally, there appear to be discontinuities in the pressures in the first 15 inches of the duct. This is particularly evident in the top wall trace. These spikes and dips in pressure are attributed to shock structure in the duct.

The data in Figure 18 has much larger uncertainty than previous figures. This trend was common in the plots with the "high pressure" data trend. This large uncertainty is due to the unsteadiness of the flow, rather than traditional uncertainty. Plans are underway for additional testing with high speed pressure transducers to record these turbulent fluctuations.

Because the embedded rocket nozzles are designed for optimum expansion at a chamber pressure around 650 psi at sea level pressure, the change in behavior of the pressure traces was initially believed to be due to the transition in plume behavior from over expanded to ideal then under expanded.[9] However in light of the dual nozzle data, It is believed that this change in behavior is due to momentum effects, as it occurs around the same mass flow for the dual and single nozzles. For the single nozzle strut, the transition occurred between chamber pressures of 600 psi and 700 psi. For the dual nozzle strut, this transition occurs around 350 psi, which was one of the chamber pressures investigated. At this pressure, both pressure distribution trends were recorded in different tests. In some tests, the transition would occur half way through the test. It is believed that humidity has an influence on the pressure trend as well. On days with high humidity, the "low pressure" data trend would be recorded at a chamber pressure of 350. However, if the humidity was low, the "high pressure" data trend would be recorded.

For the "high pressure" data trend, the duct length required for recovery to atmospheric pressure, seems to be a function of chamber pressure. This can be seen in comparing figures 17 and 18. In figure 18, the total pressure is much less than the total pressure for the single nozzle equivalent mass flow (not to be confused with static pressure in the mixing duct shown on the plot). As a result, the dual nozzle begins to recover around 15 inches downstream

of the nozzle exit, while for the single nozzle the pressure does not begin to recover until much further downstream (approximately 36 inches).

An additional trend was noted in the dual nozzle strut pressure distributions that was not seen in the single nozzle distributions. This trend occurred for mid range pressures in the dual nozzle strut (Pc = 200 psi - 300 psi). Figure 19 and 20 show the mixing duct wall pressure distributions for the single nozzle at a chamber pressure of 500 psi, and the dual nozzle at a chamber pressure of 250 psi

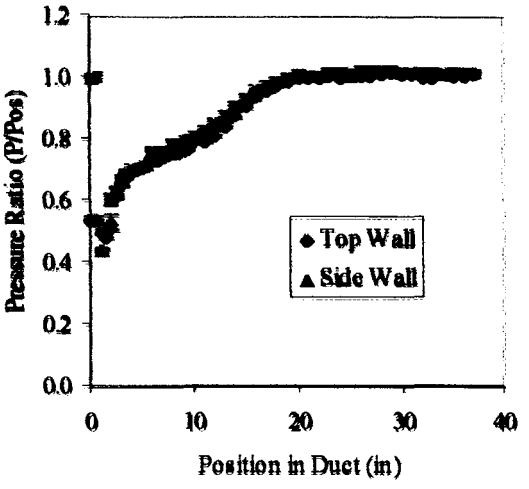

Figure 19 Single Nozzle Mixing Duct Pressure Distribution (Pc = 600 psi).

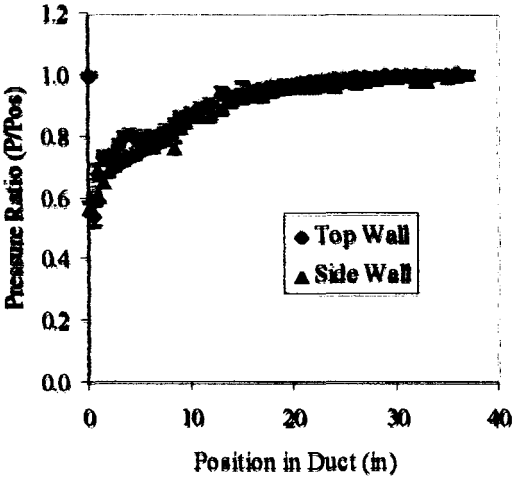

Figure 20 Dual Nozzle Mixing Duct Pressure Profile (Pc = 300 psi).

In Figure 20, there is a "hump" in the top wall pressure distribution that occurs approximately 4 inches downstream of the exit plane. This "hump" appears at 250 psi, and becomes more pronounced until the pressure distribution trend change occurs around 350 psi. This hump is not present in the single nozzle pressure profiles of equivalent mass flow, and is believed to be due to the nozzle geometry effects (2 nozzles as opposed to 1 nozzle).

VI. Conclusions

This paper presents the results of a series of tests on a single nozzle and a dual nozzle strut based ejector. The tests were conducted at various primary chamber pressure setpoints ranging from 100 to 900 psi (single nozzle) and 50 to 450 psi (dual nozle). Chamber temperature in the strut rocket was not varied other than its response to chamber pressure as an ideal gas. Lab air at atmospheric pressure was drawn through a contoured inlet into the duct. Secondary and mixing duct exit, Mach numbers were determined from Pitot-static probe measurements. Mixing duct static pressure distributions were also measured. Fluid behavior in the duct was examined with focus on mixing of the flow streams, choking mechanisms of the secondary flow stream, mass flow entrainment.

A. Mass Flow Augmentation

A choke of the secondary mass flow was demonstrated at a chamber pressure of 500 psi and 250 psi for the single and dual nozzle ejectors respectively. This corresponds to a primary mass flow of approximately 2 lbm/sec in both ejectors. From the examination of strutgap and duct wall static pressure profiles, it was concluded that the type of choke which occurs in the duct for all of the pressures examined was a mass choke rather than a traditional aerodynamic choke. Although around some chamber pressures, the pressure ratios in the strut gap region appear to approach the pressure ratio indicating an aerodynamic choke, the consistent value of the secondary mass flow which is 33% less then the theoretical value for an aerodynamic choke indicates that the mass choke is still present and that the aerodynamic choke is never truly reached.

Ratios of secondary to primary mass flow rate were investigated as a function of primary to secondary flow total pressure ratio. Secondary total pressure remained constant since the induced flow was entrained from ambient laboratory conditions. The largest mass flow augmentation occurred at the lowest primary total pressure setpoints.

As primary total pressure increased, primary and secondary mass flow both increased until the secondary mass flow choked. Primary mass flow continued to increase with increasing setpoint pressure, while secondary mass flow remained constant after the choking point. This caused the mass flow ratio to decrease sharply.

The secondary flow choked at a corresponding Mach number of 0.3 and a primary chamber pressure of approximately 500 psi (single nozzle) and 250 psi (dual nozzle). Mixing duct exit Mach number were determined and found to reach a sonic exit core flow for chamber pressures above 700 psi (single nozzle) and 350 psi (dual nozzle). In general, the exit Mach numbers were less than expected, and may be attributed to the enhanced mixing and three-dimensional effects of the asymmetric geometry, or losses in the long the mixing duct.

B. Mixing Duct Pressure Distributions

Two distinct patterns were visible in the pressure distribution plots of the mixing duct. For chamber pressures below 700 psi (single nozzle) and 350 psi (dual nozzle) the pressure traverses along the duct top and sidewalls revealed a possible top wall recirculation zone within the first 0.5 inches of the duct followed by a sharp decrease in pressure ratio. The minimum pressure ratios for the top and sidewalls decrease with increasing primary driving pressure. The sidewall pressures in the region between 5 and 10 inches exhibit a significant dip in comparison to the pressures on the top wall. This may indicate some type of local flow acceleration due to boundary layer growth. This may also be due to a different spreading rate of the supersonic core flow toward the sidewalls of the duct than toward the top and bottom walls.

For chamber pressures at or above 700 psi (single) and 350 psi (dual), the pressure traces revealed the same possible top wall recirculation zone within the first 0.5 inches of the duct followed by a sharp decrease in pressure ratio. This was followed by a more gradual pressure ratio drop to a value equal to approximately 0.3. This pressure ratio was relatively constant along the duct until a gradual recovery region occurs in which it appears the pressure ratio is trying to recover to the exit pressure. For single nozzle at the highest chamber pressures recorded, the duct does not appear to be long enough for the pressure to fully recover to atmospheric conditions. This is indication that at these high pressure ratios, the duct exhibits poor mixing between the secondary and primary flow streams. The higher chamber pressure plots also indicate the presence of shock structure in the duct evidenced by sharp discontinuities in the pressure ratios.

C. Comparison to Previous Studies

Comparisons to previous UAH PRC cold-flow mixing studies of a two-nozzle configuration provided insight into locations of suspected choking mechanisms. Mass chokes were clearly identified in the present study where they had not been in previous studies. Data was reconstructed from the twin nozzle studies in order to identify choking points. Although uncertainty information was lacking, it was concluded that the secondary flow chokes at approximately the same primary mass flow rate for both the twin and single nozzle configuration as found in the present study. However, the total pressure for the two nozzles is half that of the single nozzle. This is consistent with momentum similarity.

Results from the present study were compared to hot-fire results obtained in tests at the PSU Propulsion Engineering Research Center[12]. The PSU ejector investigations included both a single and twin strut rocket configuration. The conclusions from PSU twin thruster tests suggested that the mixing length is a function of the number of strut rockets. However, the present cold-flow study shows that the mixing length in the duct is also a significant function of primary mass flow (and hence chamber pressure). The twin rocket study at PSU shows an enhancement in the entrained mass flow over the single thruster configuration. However, in light of the present investigation of choking mechanisms, this effect is only true if the nozzles are operated below the mass addition choke threshold. Had the primary pressure of the single and twin thrusters been operated above this threshold, it is believed that entrained mass flow properties would be the same regardless of the number of thrusters employed.

VII. References

[1] Murthy, S. N. B. and Curran, E. T., High Speed Flight Propulsion Systems, *Progress in Aeronautics and Astronautics* Vol. 137, 1991.

[2] Siebenhaar, A. and Bulman, M. J., The Strutjet Engine: The Overlooked Option for Space Launch, in *31st AIAA/ASME/SAE/ASEE Joint Propulsion Conference and Exhibit* American Institute of Aeronautics and Astronautics, San Diego, California, 1995.

[3] Muller, S., Bakker, P., Hawk, C., Parkinson, D., and Turner, M., Mixing of Supersonic Jets in a Strutjet Propulsion System, *Journal of Propulsion and Power* vol. 17 (No. 5), 1129-1131, 2001.

[4] Parkinson, D., Turner, M., and Wagner, D., Mixing of Supersonic Streams, in *35th AIAA/ASME/SAE/ASEE Joint Propulsion Conference and Exhibit*Los Angeles, California, 1999.

[5] Muller, S., Hawk, C., Parkinson, D., Turner, M., and Bakker, P. G., Mixing of Supersonic Jets in a RBCC Strujet Propulsion System, in *35th AIAA/ASME/SAE/ASEE Joint Propulsion Conference and Exhibit*Los Angeles, California, 1999.

[6] Landrum, D. B., Thames, M., Parkinson, D., and Gautney, S., Investigation of the Rocket Induced Flow Field in a Rectangular Duct, in *35th AIAA/ASME/SAE/ASEE Joint Propulsion Conference and Exhibit* American Institute of Aeronautics and Astronautics, Los Angeles, California, 1999.

[7] Smith, N. T., Landrum, D. B., Hawk, C. W., and Onedera, T., Experimental Investigation of a Supersonic Non-Axisymmetric Ejector, in *10 th AIAA/NAL-NASDA-ISAS International Space Planes and Hypersonic Systems and Technologies Conference* American Institute of Aeronautics and Astronautics, Kyoto, Japan, 2001.

[8] Smith, N. T., *An Experimental Investigation of a Non-Axisymmetric Supersonic Cold-Flow Ejector*, University of Alabama in Huntsville, 2002.

[9] Lineberry, D., Landrum, D. B., Hawk, C., and Smith, N. T., Characterization of Cold Flow Non-Axisymmetric Ejectors, in *39th AIAA/ASME/SAE/ASEE Joint Propulsion Conference and Exhibit*, AIAA, Inc., Huntsville, Alabama, 2003.

[10] Fabri, J. and Siestrunck, R., *Supersonic Air Ejectors* Academic Press, New York, New York, 1958.

[11] Fabri, J. and Paulon, J., Theory and Experiments on a Supersonic Air-To Air Ejectors, 1956.

[12] Cramer, J. M., Greene, M., Pal, S., and Santoro, R. J., RBCC Ejector Mode Operating Characteristics for Single and Twin Thruster Configurations, in *37th AIAA/ASME/SAE/ASEE Joint Propulsion Conference and Exhibit* American Institute of Aeronautics and Astronautics, Salt Lake City, Utah, 2001.